A&A 633, A120 (2020)
https://doi.org/10.1051/0004-6361/201936538

Astronomy & Astrophysics

First detection of the carbon chain molecules ^{13}CCC and C^{13}CC towards SgrB2(M)⋆

T. F. Giesen[1], B. Mookerjea[2], G. W. Fuchs[1], A. A. Breier[1], D. Witsch[1], R. Simon[3], and J. Stutzki[3]

[1] Laboratory for Astrophysics, Institute of Physics, University of Kassel, Kassel 34132, Germany
e-mail: t.giesen@uni-kassel.de
[2] Tata Institute of Fundamental Research, Homi Bhabha Road, Mumbai 400005, India
[3] I. Physikalisches Institut, University of Cologne, Cologne, Germany

Received 20 August 2019 / Accepted 18 November 2019

ABSTRACT

Context. Carbon molecules and their ^{13}C-isotopologues can be used to determine the ^{12}C/^{13}C abundance ratios in stellar and interstellar objects. C_3 is a pure carbon chain molecule found in star-forming regions and in stellar shells of carbon-rich late-type stars. Latest laboratory data of ^{13}C-isotopologues of C_3 allow a selective search for the mono-substituted species ^{13}CCC and C^{13}CC based on accurate ro-vibrational frequencies.

Aims. We aim to provide the first detection of the ^{13}C-isotopologues ^{13}CCC and C^{13}CC in space and to derive the ^{12}C/^{13}C ratio of interstellar gas in the massive star-forming region SgrB2(M) near the Galactic Center.

Methods. We used the heterodyne receivers GREAT and upGREAT on board SOFIA to search for the ro-vibrational transitions $Q(2)$ and $Q(4)$ of ^{13}CCC and C^{13}CC at 1.9 THz along the line of sight towards SgrB2(M). In addition, to determine the local excitation temperature, we analyzed data from nine ro-vibrational transitions of the main isotopologue CCC in the frequency range between 1.6 and 1.9 THz, which were taken from the *Herschel* Science Data Archive.

Results. We report the first detection of the isotopologues ^{13}CCC and C^{13}CC. For both species, the ro-vibrational absorption lines $Q(2)$ and $Q(4)$ have been identified, primarily arising from the warm gas physically associated with the strong continuum source, SgrB2(M). From the available CCC ro-vibrational transitions, we derived a gas excitation temperature of $T_{\rm ex} = 44.4^{+4.7}_{-3.9}$ K, and a total column density of $N(\mathrm{CCC}) = 3.88^{+0.39}_{-0.35} \times 10^{15}$ cm^{-2}. Assuming the excitation temperatures of C^{13}CC and ^{13}CCC to be the same as for CCC, we obtained column densities of the ^{13}C-isotopologues of $N(\mathrm{C^{13}CC}) = 2.1^{+0.9}_{-0.6} \times 10^{14}$ cm^{-2} and $N(\mathrm{^{13}CCC}) = 2.4^{+1.2}_{-0.8} \times 10^{14}$ cm^{-2}. The derived ^{12}C/^{13}C abundance ratio in the C_3 molecules is 20.5 ± 4.2, which is in agreement with the elemental ratio of 20, typically observed in SgrB2(M). However, we find the $N(\mathrm{^{13}CCC})/N(\mathrm{C^{13}CC})$ ratio to be 1.2 ± 0.1, which is shifted from the statistically expected value of two. We propose that the discrepant abundance ratio arises due to the lower zero-point energy of C^{13}CC, which makes position-exchange reaction converting ^{13}CCC to C^{13}CC energetically favorable.

Key words. techniques: spectroscopic – ISM: individual objects: Sgr B2 – ISM: molecules – submillimeter: ISM – ISM: abundances – line: identification

1. Introduction

Small carbon chain molecules play an important role in the chemistry of stellar and interstellar environments since they are ubiquitous throughout the interstellar medium (Ádámkovics et al. 2003) and most likely participate in the formation of long carbon chain molecules. Furthermore, they are products of photo-fragmentation cascades of polycyclic aromatic hydrocarbons (PAHs) (Radi et al. 1988; Pety et al. 2005). Oka et al. (2003) observed the C_3 column densities to be well correlated with the corresponding C_2 column densities along several translucent lines of sight, and concluded that C_3 and C_2 are formed in the same chain of chemical reactions. However, this chemical pathway can not be used to explain the abundance of C_3 in the warm envelopes of hot cores. Post warm-up gas phase chemistry of CH_4, applicable at moderate temperatures of 30 K, is required to satisfactorily explain the abundance of C_3 and associated hydrocarbons for a few sources (Mookerjea et al. 2010, 2012, 2014). Further observations of high-density warm regions are needed to clearly establish this hypothesis of carbon chain formation in these regions.

Studies of isotope fractionation have been proven to be a useful tool for tracing chemical reaction pathways and to elucidate formation and destruction processes of interstellar molecules. At low temperatures, the isotopic ratio of molecular carbon can be significantly shifted due to small zero-point energy differences between reactants and products (e.g., Langer et al. 1984). Takano et al. (1998) were among the first to observe the three singly substituted ^{13}C-species of HC_3N and found that the abundance of HCC^{13}CN is significantly higher than those for H^{13}CCCN and HC^{13}CCN, thus indicating that the three carbon atoms are not equivalent in their formation pathways. Similar results have also been observed for CCS, CCH, C_3S, HC_3N, and c-C_3H_2 (Sakai et al. 2007, 2010, 2013; Taniguchi et al. 2016a; Yoshida et al. 2015), whereas for HC_5N, no significant difference in the abundance of the five singly substituted isotopologues was observed (Taniguchi et al. 2016b). The observed anomalies in isotopic ratios were explained by single isotope-specific reactions in the formation pathways. Based on a gas-grain chemical

⋆ A copy of the reduced spectra is available at the CDS via anonymous ftp to cdsarc.u-strasbg.fr (130.79.128.5) or via http://cdsarc.u-strasbg.fr/viz-bin/cat/J/A+A/633/A120

network, Furuya et al. (2011) confirmed that the isotope ratios of molecules, both in the gas phase and on grain surfaces, mostly depend on whether these species are formed from the carbon atom (ion) or the CO molecule. These authors concluded that the $^{12}C/^{13}C$ isotope ratio is large if the species is formed from a carbon atom, while the ratio is small if the species is formed from a CO molecule. While the evidence for isotope-specific fractionation of carbon is strongest in low-mass star-forming regions, a few instances are also seen in high-mass cores, such as G28.28-0.36 (Taniguchi et al. 2016a).

The Sagittarius B2 molecular cloud (Sgr B2) is a very massive (a few 10^6 $M_\odot$) and extremely active region of high-mass star formation, with an extraordinarily rich chemistry. It is located at a projected distance of 107 pc from Sgr A*, the compact radio source at the Galactic center and (8.34 ± 0.16) kpc away from the Sun (Reid et al. 2009). Sgr B2 contains at least two main sites of star formation, Sgr B2(N) ($\upsilon = 64$ km s^{-1}) and Sgr B2(M) ($\upsilon = 62$ km s^{-1}), which are separated by 48″. Both these sources have proven to be extremely fertile hunting grounds for complex organic molecules (Belloche et al. 2013). Owing to its strategic location and strong sub-millimeter continuum flux, Sgr B2 is one of the best suited background sources towards which absorption studies can be carried out. Because of its higher continuum temperature (Qin et al. 2008), we selected Sgr B2(M) as the background source for the detection of absorption lines of C_3 and its singly substituted ^{13}C-isotopologues.

2. Spectroscopic data

In the remainder of the paper, we use the term C_3 generally when the triatomic carbon molecule (tricarbon) is meant without considering the specific isotopic composition, and we use the terms CCC, $C^{13}CC$ and ^{13}CCC for the isotopologues $^{12}C^{12}C^{12}C$, $^{12}C^{13}C^{12}C$, and $^{13}C^{12}C^{12}C$, respectively. C_3 is a floppy linear molecule with a $^1\Sigma_g^+$ electronic ground state. As a centro-symmetric molecule, C_3 has no permanent electric dipole moment, and thus it lacks a purely rotational spectrum, but a vibrationally induced electric dipole moment allows for ro-vibrational transitions of the asymmetric stretching $\nu_3(\sigma_u)$ and the energetically low-lying bending mode $\nu_2(\pi_u)$. Matsumura et al. (1988) assigned rotationally resolved infrared spectra to the $\nu_3(\sigma_u)$ fundamental band of the CCC main isotopologue at 2040 cm^{-1} (61 THz). Later, Moazzen-Ahmadi et al. (1993) reported $\nu_3(\sigma_u)$ spectra of the ^{13}CCC isotopologue. CCC spectra of the energetically low-lying $\nu_2(\pi_u)$ mode at 63 cm^{-1} (2 THz) were published by Schmuttenmaer et al. (1990) and Gendriesch et al. (2003).

Recently, Breier et al. (2016) measured the lowest bending mode, $\nu_2(\pi_u)$, of the five singly- and multiply-substituted ^{13}C-isotoplologues of C_3. Using these accurate frequencies, we undertook an observational study of CCC, $C^{13}CC$, and ^{13}CCC to determine the $^{12}C/^{13}C$ isotopic ratio in the dense warm molecular gas along the line of sight to Sgr B2(M).

The $\nu_2(\pi_u)$ bending mode spectrum consists of *P*-, *R*- and strong *Q*-branch transitions, which are rotationally resolved. In the present analysis to derive C_3 column densities, we used a vibrational dipole moment (μ_v) of 0.432 D, which is based on the best currently available dipole moment surface (Schröder & Sebald 2016). The new value of μ_v is slightly smaller than the commonly used value of 0.437 D published by Jensen et al. (1992). For the analysis of the observed CCC, $C^{13}CC$ and ^{13}CCC lines, we used the molecular parameters obtained from our recent laboratory study (Breier et al. 2016), which also includes relevant C_3 data from the literature. Relative to the main isotopologue, CCC, the band centers of ^{13}C-substituted species are shifted toward lower frequencies, and their rotational constants are slightly smaller than those of the main isotopologue. We assume the ν_2-vibrational dipole moment of all C_3-isotopologues to be the same, which is a reasonable approximation.

A noticeable difference between the spectra of C_3-isotopologues is caused by the symmetry: in case of two identical bosonic (^{12}C: nuclear spin = 0) atoms at the end of the chain, i.e. for the case of $^{12}C^{13}C^{12}C$ or $^{12}C^{12}C^{12}C$, only even numbered *J* rotational levels exist. In contrast, for the asymmetrically substituted $^{13}C^{12}C^{12}C$ species, all *J* rotational states are present in the asymmetrically substituted ^{13}CCC. Due to the absence of every second rotational level, the values of the ro-vibrational partition functions, $Q_{\rm rv}$, of the centro-symmetric species are half as large as those of the asymmetrically substituted ^{13}CCC, which means that $Q_{\rm rv}^{\rm CCC} \approx Q_{\rm rv}^{\rm C^{13}CC} \approx 0.5 \cdot Q_{\rm rv}^{\rm ^{13}CCC}$. On the other hand, if we assume that ^{13}C is statistically distributed in C_3, we find two options to place ^{13}C, asymmetrically, at the ends of the carbon chain, but only one option to substitute the central carbon atom. Thus, there are twice as many asymmetrically substituted ^{13}CCC species as symmetrically substituted $C^{13}CC$ species, and statistically their relative abundance should be $[C^{13}CC]/[^{13}CCC] = 0.5$.

With regard to the ro-vibrational line intensities, the double excess of ^{13}CCC is compensated by the twice as large partition function $Q_{\rm rv}^{\rm ^{13}CCC}$. Thus, the line intensities of, for example, $Q(2)$ and $Q(4)$ of ^{13}CCC and $C^{13}CC$ are expected to be the same, provided that ^{13}C is purely statistically distributed, and the isotopologue abundances are not affected by any isotope-specific formation mechanism.

We calculated the Einstein $A_{\rm ul}$ coefficients in SI-units for the observed transitions using (Bernath 1995):

$$A_{\rm ul} = \frac{16\pi^3}{3\epsilon_0 h}\frac{\nu^3}{c^3}\cdot|\mu_{\rm lu}|^2 \quad \text{and} \quad |\mu_{\rm lu}|^2 = \frac{|\mu_{\rm v}|^2 L_{P/Q/R}(J)}{g_{\rm u}}, \tag{1}$$

where, $|\mu_{\rm lu}|^2$ is the square of the transition moment matrix element, and $\mu_{\rm v}$ the vibrational dipole moment. $L_{P/Q/R}(J)$ are the Hönl-London factors for *P*-, *Q*-, or *R*-type transitions for absorption from a lower $J_{\rm l}$ state, and $g_{\rm u} = 2J_{\rm u} + 1$ is the degeneracy of the upper state, $J_{\rm u}$. For ro-vibrational transitions of a linear molecule from the ground state to an degenerated first excited bending state, the Hönl-London factors are $L_P(J) = J - 1$, $L_Q(J) = 2J + 1$, and $L_R(J) = J + 2$, as given by Hansson & Watson (2005). The Einstein $A_{\rm ul}$ coefficients derived in this way are consistent with the results of the PGopher program (Western 2017) for calculating line spectra, and with the formalism for line intensities as described by Bunker & Jensen (2005). Table 1 summarizes the spectroscopic parameters for all observed transitions.

3. Observations

The observations of ^{13}CCC and $C^{13}CC$ were carried out during three flight campaigns of the SOFIA observatory with the receivers GREAT and upGREAT. In addition, we used data from the SOFIA archive and *Herschel* HEXOS data to derive a value for the gas excitation temperature $T_{\rm ex}$ of the main isotopologue CCC.

3.1. SOFIA

Observations of the $Q(2)$ and $Q(4)$ transitions of ^{13}CCC and $C^{13}CC$ were performed with the GREAT instrument in 2015 in the single-pixel configuration (Heyminck et al. 2012), and in

Table 1. Spectroscopic parameters for observed CCC, C^{13}CC, and ^{13}CCC transitions.

Transition	Frequency MHz	Einstein A_{ul} s^{-1}	E_l K	g_l	g_u
CCC					
$Q(2)$	1 890 558.188	0.01468	3.7	5	5
$Q(4)$	1 896 706.838	0.01482	12.4	9	9
$Q(6)$	1 906 337.907	0.01505	26.0	13	13
$P(2)$	1 836 823.502	0.00449	3.7	5	3
$P(4)$	1 787 890.534	0.00532	12.4	9	7
$P(6)$	1 741 122.646	0.00521	26.0	13	11
$P(8)$	1 696 525.363	0.00495	44.6	17	15
$P(10)$	1 654 087.900	0.00466	68.1	21	19
$P(12)$	1 613 805.250	0.00437	96.6	25	23
C^{13}CC					
$Q(2)$	1819596.013	0.01309	3.7	5	5
$Q(4)$	1825647.312	0.01322	12.4	9	9
^{13}CCC					
$Q(2)$	1882638.269	0.01450	3.6	5	5
$Q(4)$	1888501.880	0.01463	11.9	9	9

2016–2017 using the upGREAT array configuration (Risacher et al. 2016) onboard the Stratospheric Observatory for Infrared Astronomy (SOFIA; Young et al. 2012). The observations of ^{13}CCC were obtained during two flights of the SOFIA/GREAT flight campaigns in July 2015 and in June 2016 from New Zealand. Observations of the $Q(2)$ and $Q(4)$ transitions of C^{13}CC were performed with upGREAT/SOFIA during the New Zealand campaign in June 2017.

All observations were made in double beam-switch mode, in which the source emission is alternately placed in one of the two chopper beams, while the other beam points at off-source positions on either side of the source. This observing mode cancels the systematics related to the optical path, such as the differences in standing waves between the two chopped beams. This compensation is particularly important given the strong continuum offset of the SgrB2(M) source. The source position used for the main continuum peak on SgrB2, which is SgrB2(M), was $(\alpha_{2000}, \delta_{2000}) = (17^h47^m20\overset{s}{.}16, -28°23'04\overset{''}{.}5)$. The chopper amplitude was set to 80″, resulting in a chopper throw of 160″, which was aligned at an angle rotated counter-clockwise by 30° relative to the RA axis. The telescope pointing rms deviation, judged by the optical images on SOFIA's instrument focal plane pointing camera, as well as from the SOFIA housekeeping data, was well below 1″.

For the 2016 and 2017 observations, we used the central pixel (PX_00) of the upGREAT low-frequency arrays in both horizontal (H) and vertical (V) polarization. The stability of the V-polarization local oscillator (LO) in the June 2017 observations was marginal, resulting in an inconsistent calibration of the spectra obtained in this polarization. We therefore discarded these observations from further analysis.

In order to identify line contamination from the image side band, the observations were performed with different LO tuning offsets from the nominal setting. Table 2 lists the details of the observations, including the total integration times, T_{int}, and the rms achieved. In June 2016, observations of the ^{13}CCC $Q(4)$ line were severely affected by line contamination from the image side band. The velocity profile of the unknown and unassigned weak line from the image side band was reconstructed by shifting the observed spectra from the three tunings of July 2015 observations to the correct image-side-band velocity scale. The line profile of the line contaminating the June 2016 ^{13}CCC $Q(4)$ observations was thus determined and subtracted from the latter. The corrected June 2016 spectrum was in good agreement with the $Q(4)$ spectrum measured in the three tunings during the July 2015 campaign, so that both spectra could be averaged together, resulting in the final spectrum shown in Fig. 2.

Table 2. C^{13}CC and ^{13}CCC observational parameters for various spectral line tunings of SOFIA/GREAT (G) and upGREAT (upG) receivers.

Transition	Rec.	Obs. Date	$v_{off}^{(a)}$ km s^{-1}	T_{int} min	T_{rms} mK
^{13}CCC-$Q(2)$	G	19 July 2015	+10.0	6.8	99
^{13}CCC-$Q(4)$	G	19 July 2015	+0.0	27.9	62
	upG	9 June 2016	−10.0	12.5	96
C^{13}CC-$Q(2)$	upG	28 June 2017	0.0	5.7	112
	upG	28 June 2017	+10.0	5.1	150
C^{13}CC-$Q(4)$	upG	28 June 2017	0.0	8.5	56
	upG	28 June 2017	+10.0	2.8	150

Notes. $^{(a)}$Velocity offset of LO setting relative to the v_{LSR}.

3.2. SOFIA archives

We obtained observations of the CCC $Q(6)$ transition from the SOFIA data archive. The original observations were part of the proposal 01_151 (PI: P. Schilke, D. Neufeld). The observations were performed with GREAT on July 17, 2013 using two LO settings corresponding to offsets of 15 km s and −25 km s^{-1}, with a total integration time of 15 min. The spectrum was smoothed to a resolution of 0.2 km s^{-1} and had an rms of 10 mK.

3.3. Herschel HEXOS data

The guaranteed time key project HEXOS (Bergin et al. 2010, *Herschel* Observations of Extra-Ordinary Sources) included a full spectral survey of SgrB2(M). Here, we used the user provided data product (UPDP) for the HIFI bands 7a and 7b from the *Herschel* Science Archive in order to study all transitions, except $Q(6)$ of the CCC main isotopologue, which was taken from the SOFIA archive (see Sect. 3.2).

4. Results and analysis

Figures 1–3 show the observed spectra of all the transitions of CCC, ^{13}CCC, and C^{13}CC. Each spectrum was fitted with a single Gaussian component to obtain the velocities v_{LSR}, line widths Δv, and the integrated optical depths τ (Table 3).

The integrated optical depths of the ro-vibrational transitions were used to derive the state-specific column densities N_{J_l} of the lower state rotational levels J_l. We used Eqs. (30), (6), and (11) from Mangum & Shirley (2015) to rewrite the column density with respect to the lower state as:

$$N_{J_l} = \frac{8\pi\nu^3}{c^3}\frac{g_l}{A_{ul}\,g_u}\left[1-\exp\left(-\frac{h\nu}{k_B T_{ex}}\right)\right]^{-1}\int \tau \mathrm{d}v, \quad (2)$$

where g_l and g_u are the rotational degeneracy factors $2J+1$ of the J_l lower and J_u upper rotational level, respectively. Figure 4 shows the state-specific column densities N_{J_l} of CCC, ^{13}CCC,

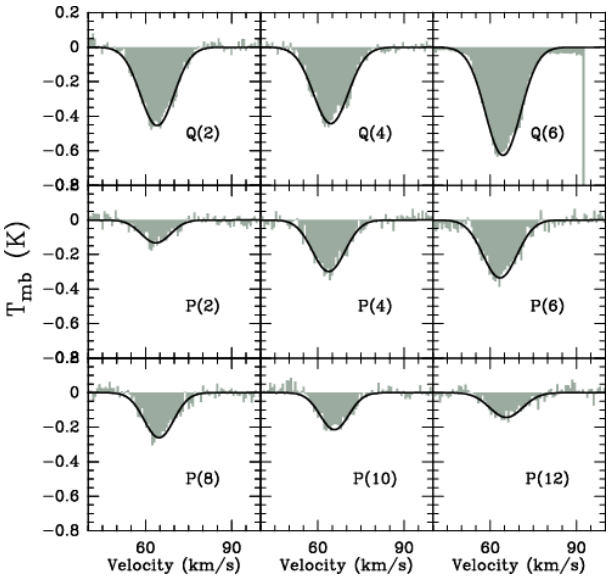

Fig. 1. Ro-vibrational spectra of CCC observed towards SgrB2(M) using HIFI/*Herschel* along with fitted Gaussian profiles (smooth curve).

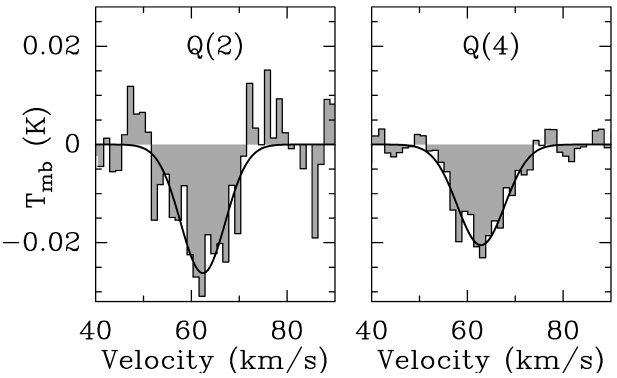

Fig. 2. Ro-vibrational spectra of ^{13}CCC observed towards SgrB2(M) using GREAT/SOFIA along with fitted Gaussian profiles (smooth curve).

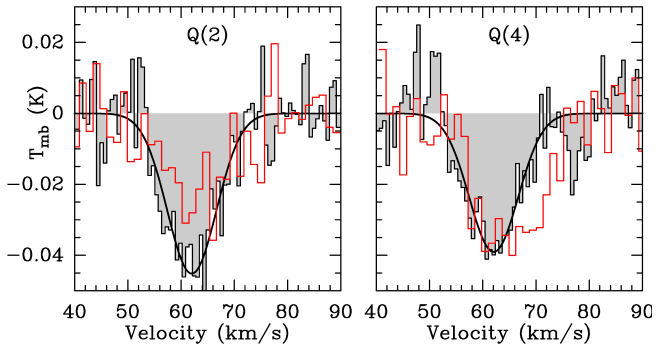

Fig. 3. Ro-vibrational spectra of C^{13}CC observed towards SgrB2(M) using upGREAT/SOFIA along with fitted Gaussian profiles (smooth curve). The H-polarization is shown as filled spectrum, and the V-polarization as red spectrum.

and C^{13}CC as a Boltzmann plot, where we used the CCC column densities to derive the gas excitation temperature $T_{\rm ex}$. Since the state-specific column density itself is a function of temperature (Eq. (2)), we used an iterative fitting procedure until the temperature converged to the final value of $T_{\rm ex} = 44.4^{+4.7}_{-3.9}$ K. It should be noted that for $J_{\rm l} = 2$, 4, 6 of CCC, where both, $P(J)$ and $Q(J)$

Table 3. Summary of observed and derived quantities for the CCC, C^{13}CC, and ^{13}CCC transitions.

	$\tau_{\rm peak}$	$\upsilon_{\rm LSR}$ km s^{-1}	$\Delta\upsilon$ km s^{-1}	$\int \tau {\rm d}\upsilon$ km s^{-1}	$N_{J_{\rm l}} \times 10^{13}$ cm^{-2}
CCC					
$Q(2)$	0.53	63.9(1)	11.6(2)	6.6(1)	32.6(5)
$Q(4)$	0.56	64.4(1)	13.7(2)	8.3(1)	40.9(5)
$Q(6)$	0.87	64.3(1)	12.5(1)	11.5(1)	56.6(5)
$P(2)$	0.15	63.5(3)	12.7(8)	2.0(1)	49.8(25)
$P(4)$	0.34	63.8(1)	12.5(3)	4.5(1)	67.8(15)
$P(6)$	0.39	63.4(1)	12.5(3)	5.2(1)	68.5(13)
$P(8)$	0.31	64.4(1)	13.0(4)	4.2(1)	52.1(12)
$P(10)$	0.24	65.7(2)	11.7(4)	2.9(1)	34.9(12)
$P(12)$	0.15	65.5(4)	13.0(8)	2.1(1)	24.8(12)
C^{13}CC [(a)]					
$Q(2)$	0.046	62.0(3)	10.8(7)	0.53(3)	2.64(15)
$Q(4)$	0.040	62.0(4)	10.8(10)	0.46(4)	2.28(20)
^{13}CCC					
$Q(2)$	0.027	62.8(8)	11.1(15)	0.32(4)	1.58(20)
$Q(4)$	0.021	62.9(3)	11.6(6)	0.26(1)	1.26(5)

Notes. [(a)]Only H-polarization data was used.

transitions have been observed, the column densities of P-branch lines are consistently higher than those of the Q-branch lines, which significantly contributes to the obtained uncertainties of $T_{\rm ex}$. A similar trend has been seen for previous CCC observations from other sources (Mookerjea et al. 2010, 2012, 2014), however the reason behind this is not clear.

In Fig. 4, we also present the state-specific column densities $\log(N_0)$ of $J_{\rm l} = 0$ rotational states. The values for C^{13}CC and ^{13}CCC were obtained from a Boltzmann fit to $Q(2)$ and $Q(4)$, and under the assumption that the excitation temperatures of C^{13}CC and ^{13}CCC, and thus the slopes of the Boltzmann plots, are the same as for CCC. Within limits of uncertainties shown by the shaded zone in Fig. 4, the state-specific column densities of C^{13}CC are found to be systematically larger than those of ^{13}CCC. This can also be seen from Figs. 2 and 3, where line intensities of C^{13}CC are stronger than those of ^{13}CCC.

We calculated the total column densities N of the three C_3-isotopologues by using the partition functions $Q_{\rm rv}$ given in Eq. (3). Due to spin statistics half the rotational levels of the symmetric molecules CCC and C^{13}CC are missing, whereas for the asymmetric ^{13}CCC, all rotational states are present. Hence, the partition function $Q_{\rm rv}$ of the asymmetric molecule ^{13}CCC is twice as large as those of the symmetric molecules (Table 4). At 44 K, the lowest bending states $v_2 = 1$ ($E_1 = 90.6$ K) and $v_2 = 2$ ($E_2 = 191.4$ K) are thermally populated, and the contributions of $v_2 = 0$, 1, 2 to the partition functions are 77, 19 and 4%, respectively. Therefore, in Eq. (3), we took vibrational excitation up to $v_2 = 2$ into account, but ignored higher vibrational levels. The ro-vibrational energy levels $E_{\rm rv}$ were calculated using the molecular parameters of Breier et al. (2016), and with $g_v = 1$, 2, 3, the degeneracy factors of the bending states $v_2 = 0$, 1, 2, respectively.

$$Q_{\rm rv} = \sum_{J_{\rm l}({\rm v}=0,1,2)} (2J_{\rm l}+1)\, g_{\rm v} \exp\left(\frac{-E_{\rm rv}(J_{\rm l},{\rm v})}{k_{\rm B} T_{\rm ex}}\right). \quad (3)$$

We used Eq. (4) to calculate the total column densities of CCC, C^{13}CC and ^{13}CCC, the results of which are presented

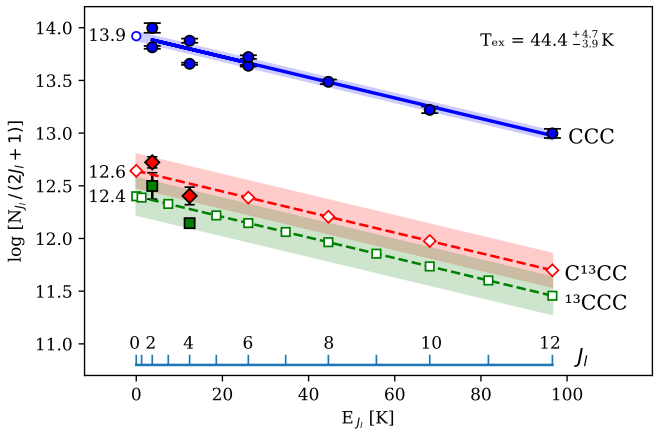

Fig. 4. Rotation diagram for C_3 lines observed with SOFIA/GREAT, upGREAT and with HIFI/*Herschel* towards SgrB2(M). The excitation temperature, $T_{ex} = 44.4^{+4.7}_{-3.9}$ K, was derived from a linear fit to the state-specific column densities N_l (J_l = 2, 4, ...12) of the main isotopologue, CCC (blue solid line and blue shaded $\pm 1\sigma$ error range). A straight line with the temperature slope of the main isotopologue was fitted to the data J_l = 2, 4 of the isotopologues C^{13}CC (red) and ^{13}CCC (green). Filled symbols represent measured values, empty symbols are obtained from the least-squares fit. Note, the centro-symmetric species, CCC and C^{13}CC, only have even-numbered J_l levels. The numbers to the left are the log (N_0) values for J_l = 0 obtained from the fit.

Table 4. Total column densities and partition functions of CCC, C^{13}CC and ^{13}CCC transitions.

	T_{ex}(K)	log (N_0)	Q_{rv}	$N \times 10^{14}$ cm^{-2}	rel.
CCC	$44.4^{+4.7}_{-3.9}$	13.92(04)	46.64	$38.8^{+3.9}_{-3.5}$	100%
C^{13}CC	44.4 [a]	12.64(16) [b]	47.66	$2.1^{+0.9}_{-0.6}$ [b]	5 ± 2%
^{13}CCC	44.4 [a]	12.40(18) [b]	97.30	$2.4^{+1.2}_{-0.8}$ [b]	6 ± 3%

Notes. [a]T_{ex} is fixed to the value derived for CCC. [b]Uncertainties are given as mean absolute deviation (MAD) of the two measured $Q(2)$ and $Q(4)$ column densities from their mean value.

in Table 4.

$$N = Q_{rv} \frac{N_{J_l}}{2J_l + 1} \exp\left(\frac{E_{rot}(J_l)}{k_B T_{ex}}\right) \quad (4)$$

For the main isotopologue, we obtained a total column density of N(CCC) = $38.8^{+3.9}_{-3.5} \times 10^{14}$ cm^{-2}, the uncertainty of which is mainly due to the uncertainty of the excitation temperature T_{ex}. The CCC column density is in agreement with the value derived by Polehampton et al. (2007) based on ISO/LWS observations. For the two ^{13}C-isotopologues, we derived the column densities N(C^{13}CC) = $2.1^{+0.9}_{-0.6} \times 10^{14}$ cm^{-2} and N(^{13}CCC) = $2.4^{+1.2}_{-0.8} \times 10^{14}$ cm^{-2}. The single-state column densities of $Q(2)$ and $Q(4)$ deviate by more than the $\pm 1\sigma$ error bars from the 44 K temperature curve (Fig. 4). To give a more realistic error for the total column densities N(^{13}CCC) and N(C^{13}CC), we used the mean absolute deviation (MAD) of the $Q(2)$ and $Q(4)$ column densities as uncertainties of the ^{13}CCC and C^{13}CC total column densities. With regard to the main isotopologue, CCC, the relative abundances of C^{13}CC and ^{13}CCC are 5 and 6%, respectively, and both have large uncertainties (see Table 4).

5. Discussion

In the previous section, we gave the total column densities of the isotopologues CCC, ^{13}CCC, and C^{13}CC, from which the relative abundances $N(a)/N(b)$, with a, b representing two of the three observed isotopologues, can be derived. Furthermore, we aim to obtain a value for the ^{12}C/^{13}C atomic carbon ratio present in C_3 molecules of the Galactic center, which then can be compared to results obtained for other carbon-containing molecules and their mono-substituted ^{13}C isotopologues. The $N(a)/N(b)$ ratios can be calculated directly from the total column densities N listed in Table 4, and the ^{12}C/^{13}C ratio can be derived from:

$$\frac{^{12}C}{^{13}C} = \frac{3\,N(CCC)}{N(^{13}CCC) + N(C^{13}CC)}. \quad (5)$$

The ratios $N(a)/N(b)$ obtained from the total column densities are listed in Table 5 as TOTAL, and the corresponding ^{12}C/^{13}C ratio is given at the end of the row. The large errors of up to 50% are mainly due to the uncertainties of the ^{13}CCC and C^{13}CC total column densities given in Table 4. As an alternative method, the $N(a)/N(b)$ ratios can be calculated from single state-specific column densities $N^a_{J_l}$ and $N^b_{J_l}$ of the isotopologues a and b via Eq. (4):

$$\frac{N(a)}{N(b)} = \frac{Q^a_{rv}\, N^a_{J_l}\, (2J^b_l + 1)}{Q^b_{rv}\, N^b_{J_l}\, (2J^a_l + 1)} \cdot \exp\left(\frac{\Delta E_{rot}}{k_B T_{ex}}\right), \quad (6)$$

with the energy difference ΔE_{rot} of the rotational levels J^a_l and J^b_l. If for both isotopologues the same rotational state, $J^a_l = J^b_l$ is chosen, then ΔE_{rot} is close to zero and can be neglected. In our analysis, we calculated the ratios for $Q(2)$ and $Q(4)$ separately using the state-specific column densities given in Table 3. Similar to Eq. (5), the ^{12}C/^{13}C isotope ratio of C_3 can be calculated from Eq. (7), neglecting the small energy differences between rotational levels of identical quantum numbers J_l of the three isotopologues:

$$\frac{^{12}C}{^{13}C} \approx \frac{3\, Q^{CCC}_{rv}\, N_{J_l}(CCC)}{Q^{^{13}CCC}_{rv}\, N_{J_l}(^{13}CCC) + Q^{C^{13}CC}_{rv}\, N_{J_l}(C^{13}CC)}. \quad (7)$$

The ratios $N(a)/N(b)$ derived from state-specific column densities of $Q(2)$ and $Q(4)$ via Eq. (6), as well as the corresponding ^{12}C/^{13}C ratios calculated from Eq. (7), are listed in Table 5. It should be noted that the given uncertainties are a result of the small uncertainties of the $Q(2)$ and $Q(4)$ state-specific column densities, which do not depend on the temperature T_{ex}. Nevertheless, the ratios derived from $Q(2)$ and $Q(4)$ should agree within the error bars if thermal equilibrium is assumed. We found that the results for $Q(2)$ and $Q(4)$ differ significantly, and concluded that their uncertainties are largely underestimated. Therefore, in Table 5, we give the mean values of $Q(2)$ and $Q(4)$ as $N(a)/N(b)$ AV, and their mean absolute deviations (MAD) in brackets. Table 5 also presents the expected values $N(a)/N(b)$ (EXPEC) for an assumed ^{12}C/^{13}C ratio of 20, the value typically found for gas near the Galactic Center.

We conclude that the derived averaged (AV) ^{12}C/^{13}C ratio of 20.5 ± 4.2 is in good agreement with the statistically expected ratio of 20. The averaged value (AV) N(CCC)/N(^{13}CCC) = 12.7 ± 2.8 is larger than the expected value of 10, but both values agree within error bars. On the contrary, the ratio N(CCC)/N(C^{13}CC) = 14.8 ± 2.7 is significantly smaller than the expected value of 20, which indicates a moderate enhancement of the symmetric species, C^{13}CC. Accordingly, the ratio

Table 5. Derived $^{12}C/^{13}C$ ratios in C_3 and fractional abundances of C_3 isotopologues.

N^a/N^b	$\frac{N(CCC)}{N(C^{13}CC)}$	$\frac{N(CCC)}{N(^{13}CCC)}$	$\frac{N(^{13}CCC)}{N(C^{13}CC)}$	$\frac{^{12}C}{^{13}C}$
TOTAL	18.6(7.0)	16.0(6.7)	1.2(0.6)	25.8(7.5)
$Q(2)$	12.1(0.7)	9.9(1.3)	1.2(0.2)	16.3(1.2)
$Q(4)$	17.6(1.6)	15.6(0.6)	1.1(0.1)	24.7(1.2)
AV	14.8(2.7) [a]	12.7(2.8) [a]	1.2(0.1) [a]	20.5(4.2) [a]
EXPEC	20	10	2	20

Notes. The $\pm1\sigma$ standard deviations are given in brackets. TOTAL: calculated from total column densities N given in Table 4. $Q(2)$, $Q(4)$: calculated via Eq. (6) from N_{J_l} values in Table 3. AV [a]: mean of $Q(2)$ and $Q(4)$ and mean absolute deviations (MAD). EXPEC: statistically expected values for $^{12}C/^{13}C = 20$.

$N(^{13}CCC)/N(C^{13}CC) = 1.2 \pm 0.1$ is smaller than the statistically expected value of two. This isotopic shift in favor of the centrally substituted species $C^{13}CC$ can be explained either by a less effective formation of ^{13}CCC, or by isotope position-exchange reactions. In Eq. (8), the reactant $X(^{12}C)$ can be, for example, C^+, or any carbon molecule or molecular ion that exchanges a ^{12}C carbon atom and thus changes the ordering of carbon atoms in the C_3 molecule

$$X(^{12}C) + {}^{13}CCC \rightleftharpoons C^{13}CC + X(^{12}C) + \Delta E_0. \quad (8)$$

For Eq. (8), the equilibrium is determined by the constant k_p of a chemical reaction:

$$k_p = \exp\left(\frac{-\Delta G}{k_B\, T_{ex}}\right) = \frac{Q^{\,^{13}CCC}}{Q^{\,C^{13}CC}} \exp\left(\frac{-\Delta E_0}{k_B\, T_{ex}}\right). \quad (9)$$

Here, ΔG and ΔE_0 are the differences in Gibbs energy and the zero point energy, respectively. We used calculated vibrational energies of the C_3-isotopologues published by Schröder & Sebald (2016) to calculate accurate zero point energies. We found that $C^{13}CC$ has a zero point energy smaller by 15.9 K than ^{13}CCC, and hence, $C^{13}CC$ is more stable than ^{13}CCC. At high excitation temperatures, the reaction constant k_p converges to the ratio of the partition functions, which equals two (as obtained from a statistical distribution of isotopes). On the other hand, at an excitation temperature of 44 K, the value of k_p is reduced by a factor of 0.7, which leads to an expected abundance ratio of $N(^{13}CCC)/N(C^{13}CC) = 1.4$, a result which is very close to very close to the observed value of 1.2 ± 0.1. It should be noted that the equilibrium of Eq. (8) only depends on the amount of ^{12}C, but is independent of the available ^{13}C budget.

Furthermore, as has extensively been studied in case of ozone, O_3, the reaction rate that leads to the formation of the symmetric isotopologue can significantly differ from the reaction rate that forms the asymmetric species, see, for example (Feilberg et al. 2013). A review of mass-independent isotope effects in chemical reactions was published by Thiemens (2006). In general, the symmetry effect in rate coefficients depends on the spin statistical weights, as was explained in case of ozone by Gellene (1996). It is largest for nuclei of zero spin, when half of the molecular states are missing for spin statistical reasons, as is the case for ^{16}O in reaction with ^{18}O. The symmetry effect may also be relevant for ^{12}C in reaction with ^{13}C, but to our knowledge this has not yet been considered in the formation process of C_3.

Till now, the abundance of C_3 in the warm envelopes of hot cores has been consistently explained in terms of chemical pathways involving post-warm-up gas phase chemistry of CH_4 released from grain surfaces (Mookerjea et al. 2012). This warm carbon-chain chemistry (WCCC) network also forms molecules like CCH, c-C_3H_2, CH_3CCH, HC_3N, CH_3CN, etc. (Mookerjea et al. 2012). Based on a spectral line survey with IRAM 30 m telescope, Belloche et al. (2013) derived the column densities of CO and several hydrocarbons including, for example, CCH, CH_3CCH, c-C_3H_2, CH_3CN, HC_3N, and their multiple ^{13}C isotopologues. In this analysis, the authors derived a multi-component global fit to the spectrum assuming local thermodynamic equilibrium (LTE) and found that for all these species, including CO, the $^{12}C/^{13}C$ ratio is ~20. For the molecules CCH, CH_3CCH, c-C_3H_2, CH_3CN, and HC_3N, the $^{12}C/^{13}C$ ratio is 20, 17, 20, 12, and 13, respectively, which, within the limits of uncertainties, is consistent with our finding based on C_3. However, in contrast to our findings for C_3 and its isotopologues, the isotopic ratio in all these molecules in SgrB2(M) is identical irrespective of the position of the isotope-substituted carbon atom in the molecule.

The non-equivalence of ^{13}C-substitution in carbon-chain molecules have also been observed in dark clouds, low-mass star forming regions as well as in hot cores. Sakai et al. (2010) determined the $[C^{13}CH]/[^{13}CCH]$ ratio for the dark cloud TMC-1 and the low-mass star forming core L1527 to be ~1.6, and Taniguchi et al. (2016a) observed all three ^{13}C isotopologues of HC_3N in the hot core G28.28-0.36, and found that $HCC^{13}CN$ is more abundant by a factor of 1.4 compared to the other two equally abundant isotopologues. These authors explained the difference in abundances of the different isotopomers in terms of the formation pathway involving neutral–neutral reaction for the respective molecular species. Additionally, Furuya et al. (2011) pointed out that because of the difference in zero-point vibrational energy of the end-substituted and centrally substituted species like CCH and CCS, it is also possible to have an exchange of the ^{13}C position by isotopomer-exchange reaction.

Yoshida et al. (2015) studied the isotopic abundances of c-C_3H_2 in L1527 and found for c-C_3H_2 that the symmetric species c-$CC^{13}CH_2$ with a lower zero-point energy has a larger abundance than the asymmetric c-$C^{13}CCH_2$ species. Yoshida et al. (2015) suggested position-exchange reactions as a possible mechanism of the relative enrichment of one of the isotopologues. Among all these molecules, C_3 is closest to c-C_3H_2, since both molecules contain three carbon atoms, of which two are equivalent and are formed in dense clouds via WCCC, and, furthermore, the two molecules show similar trends in abundances of ^{12}C and ^{13}C species.

6. Summary

We present the first detection of the singly-substituted ^{13}C-isotopologues ^{13}CCC and $C^{13}CC$, along with nine ro-vibrational transitions of the main isotopologue, CCC, towards the high-mass star forming core, SgrB2(M). All the transitions are detected in absorption and around velocities of 62–64 km s^{-1}, suggesting that the absorption features are due to warm molecular gas physically associated with the background source. We estimate a rotational temperature of 44.4 K to explain the optical depths of all the observed transitions of C_3 assuming LTE. The column densities for CCC, ^{13}CCC, and $C^{13}CC$ were estimated considering the excitation temperatures of all the species to be identical and assuming LTE. We find that the $^{12}C/^{13}C$ abundance ratio in C_3 is 20.5 ± 4.2, which is in agreement with

the observed atomic ratio of 20 in SgrB2(M). We find the $N(^{13}CCC)/N(C^{13}CC)$ ratio to be 1.2 ± 0.1, as opposed to the statistically expected value of two, and we propose that this discrepancy arises due to the lower zero-point energy of C^{13}CC, which makes position-exchange reaction converting ^{13}CCC to C^{13}CC energetically favorable.

Acknowledgements. GREAT is a development by the MPI für Radioastronomie and KOSMA/Universität zu Köln, in cooperation with the DLR Institut für Optische Sensorsysteme. The development of GREAT is financed by the participating institutes, by the German Aerospace Center (DLR) under grants 50 OK 1102, 1103 and 1104, and within the Collaborative Research Centre 956, funded by the Deutsche Forschungsgemeinschaft (DFG). T.F.G. was supported by project B2 within CRC 956; A.A.B. and T.F.G. were supported by DFG SPP-ISM 1573. The work by R.S. and J.S. was supported by project A4 within CRC 956; B. Mookerjea received travel support as a visiting scientist from CRC 956. SOFIA is jointly operated by the Universities Space Research Association, Inc. (USRA), under NASA contract NAS2-97001, and the Deutsches SOFIA Institut (DSI) under DLR contract 50 OK 0901 and 50 OK 1301 to the University of Stuttgart. We thank the SOFIA operations and engineering teams for their dedication and supportive response.

References

Ádámkovics, M., Blake, G. A., & McCall, B. J. 2003, ApJ, 595, 235
Belloche, A., Müller, H. S. P., Menten, K. M., Schilke, P., & Comito, C. 2013, A&A, 559, A47
Bergin, E. A., Phillips, T. G., Comito, C., et al. 2010, A&A, 521, L20
Bernath, P. F. 1995, Spectra of Atoms and Molecules (Oxford, UK: Oxford University Press)
Breier, A. A., Büchling, T., Schnierer, R., et al. 2016, J. Chem. Phys., 145, 234302
Bunker, P. R., & Jensen, P. 2005, Molecular Symmetry and Spectroscopy (Canada: NRC Research Press)
Feilberg, K. L., Wiegel, A. A., & Boering, K. A. 2013, Chem. Phys. Lett., 556, 1
Furuya, K., Aikawa, Y., Sakai, N., & Yamamoto, S. 2011, ApJ, 731, 38
Gendriesch, R., Pehl, T. F., Winnewisser, G., & Lewen, F. 2003, Z. Naturforsch., 58a, 129
Gellene, G. I. 1996, Science, 274, 1344
Hansson, A., & Watson, J. K. G. 2005, J. Mol. Spectr., 233, 169
Heyminck, S., Graf, U. U., Güsten, R., et al. 2012, A&A, 542, L1
Jensen, P., Rohlfing, C. M., & Almloef, J. 1992, J. Chem. Phys., 97, 3399
Langer, W. D., Graedel, T. E., Frerking, M. A., & Armentrout, P. B. 1984, ApJ, 277, 581
Mangum, J. G., & Shirley, Y. L. 2015, PASP 127, 266
Matsumura, K., Sawaraku, N., Kanamori, H., Kawaguchi, K., & Hirota, E. 1988, J. Chem. Phys. 89, 3491
Moazzen-Ahmadi, N., & McKellar, A. R. W. 1993, J. Chem. Phys., 98, 7757
Mookerjea, B., Giesen, T., Stutzki, J., et al. 2010, A&A, 521, L13
Mookerjea, B., Hassel, G. E., Gerin, M., et al. 2012, A&A, 546, A75
Mookerjea, B., Vastel, C., Hassel, G. E., et al. 2014, A&A, 566, A61
Oka, T., Thorburn, J. A., McCall, B. J., et al., 2003, ApJ, 582, 823
Pety, J., Teyssier, D., Fossé, D., et al. 2005, A&A, 435, 885
Polehampton, E. T., Baluteau, J.-P., Swinyard, B. M., et al. 2007, MNRAS, 377, 1122
Qin, S.-L., Zhao, J.-H., Moran, J. M., et al. 2008, ApJ, 677, 353
Radi, P. P., Bunn, T. L., Kemper, P. R., Molchan, M. E., & Bowers, M. T. 1988, J. Chem. Phys., 88, 2809
Reid, M. J., Menten, K. M., Zheng, X. W., Brunthaler, A., & Xu, Y. 2009, ApJ, 705, 1548
Risacher, C., Güsten, R., & Stutzki, J., et al. 2016, A&A, 595, A34
Sakai, N., Ikeda, M., Morita, M., et al. 2007, ApJ, 663, 1174
Sakai, N., Saruwatari, O., Sakai, T., Takano, S., & Yamamoto, S. 2010, A&A, 512, A31
Sakai, N., Takano, S., Sakai, T., et al. 2013, J. Phys. Chem. A, 117, 9831
Schmuttenmaer, C. A., Cohen, R. C., Pugliano, N., et al. 1990, Science, 249, 897
Schröder, B., Sebald, P. 2016, J. Chem. Phys., 144, 044307
Takano, S., Masuda, A., Hirahara, Y., et al. 1998, A&A, 329, 1156
Taniguchi, K., Saito, M., & Ozeki, H. 2016a, ApJ, 830, 106
Taniguchi, K., Ozeki, H., Saito, M., et al. 2016b, ApJ, 817, 147
Thiemens, M. H. 2006 Ann. Rev. Earth Planet Sci., 34, 217
Western, C. M. 2017, J. Quant. Spectr. Rad. Transf., 186, 221
Yoshida, K., Sakai, N., Tokudome, T., et al. 2015, ApJ, 807, 66
Young, E. T., Becklin, E. E., Marcum, P. M., et al. 2012, ApJ, 749, L17